Unsteady Convective Flow of a Reactive Heat-Generating/Absorbing Fluid in a Vertical Tube with Ramped Temperature and Concentration Boundaries under Diffusion-Thermo Effects

Sylvester Bakut Joseph
Department of Mathematics and Statistics, Nuhu Bamalli Polytechnic, Zaria, Nigeria

Abstract
This study investigates the impact of diffusion-thermo coupling on the transient natural convection of a chemically reactive viscous fluid. The fluid experiences internal heat generation or absorption while flowing through an infinite vertical tube that is subjected to both ramped wall heating and concentration conditions. To analyze this system, the governing transport equations have been transformed using the Laplace technique and solved analytically, expressing the solutions in terms of modified Bessel functions. These equations were then numerically inverted using a Riemann sum approximation to handle the complexities associated with exact inversion. The results are presented for representative fluid properties and system parameters, highlighting the evolution of velocity, temperature, concentration, and associated transfer rates such as Nusselt and Sherwood numbers, as well as skin friction. In addition, steady-state solutions have been derived in closed form, and their convergence with the transient solutions at large time scales has been confirmed. These findings provide valuable insights into the thermofluidic behavior relevant to advanced thermal management, energy systems, and chemically reactive transport processes, particularly where ramped boundary heating plays a crucial role.

Keywords: chemical reaction; ramped; isothermal; diffusion thermo; Riemann sum; heat source/sink; tube.

Introduction:
The study of buoyancy-driven flow in vertical cylindrical domains has attracted considerable attention in thermal sciences because such geometries are widely encountered in industrial and natural systems. Vertical tubes and cylinders are frequently used in heat exchangers, chemical reactors, cooling rods, and biomedical devices where the interaction between temperature and solute gradients drives convective currents. Unlike flat or annular geometries, cylindrical confinement produces distinct radial variations and boundary layer structures. The onset and development of convection in such systems is time-dependent, especially during operational transients such as start-up or load changes. For this reason, transient models provide more realistic insight into performance and stability than steady-state approximations (Ganesan & Rani, 1998; Rani, 2003; Paul, et al., 2017).
An important extension to conventional boundary conditions is the introduction of ramped temperature or ramped concentration at the wall, which better reflects practical conditions where heating and solute addition occur gradually rather than instantaneously. Studies in vertical tubes with ramped heating have demonstrated that such conditions significantly alter the rate of boundary layer growth and the time required to reach quasi-steady behavior (Jha & Oni, 2016; Jha, et al., 2024). When ramped temperature is combined with ramped surface concentration, the convective fields become even more complex, as solutal buoyancy interacts with thermal buoyancy in a time-dependent fashion. Work by Vanita and Kumar (2016) confirmed that

https://doi.org/10.5281/zenodo.17252081

combining ramped wall conditions with external magnetic fields yields outcomes that differ substantially from constant boundary cases. These investigations underline the need for including ramped thermal and solutal conditions in transient cylinder models to improve predictive accuracy for real processes.

Reactive fluids introduce additional complexity since chemical reactions may release or absorb energy and therefore alter local buoyancy. Early studies in vertical cylinders established that even simple first-order reactions have strong impacts on transient velocity and concentration fields (Jha, et al., 2011). Subsequent research expanded this by showing that coupling chemical kinetics with internal heat generation or absorption significantly changes the nature of convective development (Jha, et al., 2022a, 2022b). For instance, endothermic reactions or heat sinks can slow the rate at which flows evolve, while exothermic reactions or heat sources accelerate convection. Similar conclusions have been reached in magneto-nanofluid and radiation-based models where reactive terms were incorporated (Machireddy, 2013; Chamkha et al., 2011; Dwivedi et al., 2023). Such outcomes illustrate why it is essential to consider the simultaneous influence of chemical reaction and heat source–sink mechanisms in transient convection studies.

Another factor that cannot be ignored in multicomponent systems is cross-diffusion. The Soret effect leads to mass fluxes caused by temperature gradients, while the Dufour effect represents the reverse phenomenon where concentration gradients drive energy flux. Although often omitted in simplified models, investigations around vertical cylinders have shown that these terms can markedly influence the overall transport process. Numerical analyses demonstrated that heat and mass transfer rates can be misrepresented if Dufour and Soret terms are excluded (Rani & Kim, 2009). Other contributions confirmed that the inclusion of cross-diffusion significantly alters boundary layer thickness, particularly in porous media or non-Newtonian fluids (Cheng, 2010; Rani & Reddy, 2013). More recent work with nanofluids and deformable cylinders reinforced this, showing that activation energy and variable wall conditions magnify the role of Dufour and Soret effects (Shaheen et al., 2021; Jagan & Sivasankaran, 2022). Hence, any attempt to construct a comprehensive framework for transient convection in vertical cylinders must include cross-diffusion phenomena alongside heat and mass transfer.

The sensitivity of vertical cylinder convection to boundary variability has been established across a wide range of scenarios. Oscillating cylinders, stratified surroundings, or ramped wall inputs all create distinct transient signatures. Investigations into oscillating cylinders showed that unsteady wall motion significantly affects energy transport (Khan, et al., 2018). Studies in stratified environments demonstrated how ambient density variations influence stabilization times (Deka & Paul, 2012; Paul et al., 2017). Other research examined constant heat flux or accelerated cylinder motion, revealing how these conditions affect momentum and heat transfer (Deka et al., 2017; Deka et al., 2014). Alongside these, magnetic fields, viscoelastic effects, porous media, and radiation have been incorporated, showing that the vertical cylinder geometry is a useful testbed for integrating multiple physical processes (Mahato, et al., 2021; Dwivedi, et al., 2020, 2021; Sravanthi, et al., 2018; Alharbi, et al., 2023).

Despite the progress made, current models often address these influences in isolation. Very few studies have attempted to simultaneously treat ramped wall temperature, ramped surface concentration, chemical reactivity, internal heat generation or absorption, and Dufour effects in the same cylindrical framework. Yet, these are precisely the conditions encountered in real-world processes such as chemical reactors, catalytic converters, and tubular biomedical devices. A unified analysis of these combined mechanisms is essential for advancing predictive capability and for supporting the design of systems where transient behavior

https://doi.org/10.5281/zenodo.17252081

governs performance. This motivates the present study, which develops a model for transient natural convection in a vertical cylinder under ramped wall temperature and ramped surface concentration, with explicit inclusion of reactive fluids, heat generation or absorption, and Dufour effects.

Mathematical analysis:

Consider a vertical tube of infinite length, having a radius r_0 through which a viscous incompressible fluid flows. The tube axis is the $z^/$-axis, and the $r^/$- axis is perpendicular to it. Figure 1 shows the physical configuration. When $t^/ \leq 0$, the temperature and concentration of the tube wall and the fluid are the same and given by T_0 and C_0, respectively, where $t^/$ is the dimensional time. For$t^/ > 0$, the wall of the tube is subjected to ramped wall temperature $T_0 + \frac{(T_w - T_0)t^/\nu}{{r_0}^2\zeta_1}$ and ramped surface concentration $C_0 + \frac{(C_w - C_0)t^/\nu}{{r_0}^2\zeta_1}$ when $t^/ \leq \frac{{r_0}^2\zeta_1}{\nu}$ after which they become constant functions T_w and C_w when$t^/ > \frac{{r_0}^2\zeta_1}{\nu}$. The symbol ζ_1 is a reference time chosen arbitrarily, while T_w and C_w are the temperature and concentration after time$t^{'}$. It is assumed that heat generation/absorption of the form $Q_0(T^/ - T_0)$ exists in the fluid, where Q_0 is the dimensional heat generation/absorption parameter and $T^/$ is the dimensional temperature. It is also assumed that the fluid undergoes a chemical reaction of the form $K^/(C^/ - C_0)$ where $K^/$ is the dimensional chemical reaction parameter and $C^/$ is the dimensional concentration. Additionally, the flow is subjected to the Diffusion thermo (Dufour) effect. When the Boussinesq approximation is applied with the above assumptions, the model in dimensional form is given as:

$$\frac{\partial u^/}{\partial t^/} = \nu\frac{1}{r^/}\frac{\partial}{\partial r^/}\left(r^/\frac{\partial u^/}{\partial r^/}\right) + g\beta^*(T^/ - T_0) + g\beta(C^/ - C_0) \quad (1)$$

$$\frac{\partial T^/}{\partial t^/} = \alpha\frac{1}{r^/}\frac{\partial}{\partial r^/}\left(r^/\frac{\partial T^/}{\partial r^/}\right) + D_C\frac{1}{r^/}\frac{\partial}{\partial r^/}\left(r^/\frac{\partial C^/}{\partial r^/}\right) - \frac{Q_0}{\rho C_p}(T^/ - T_0) \quad (2)$$

$$\frac{\partial C^/}{\partial t^/} = D\frac{1}{r^/}\frac{\partial}{\partial r^/}\left(r^/\frac{\partial C^/}{\partial r^/}\right) - K^/(C^/ - C_0)$$

In the above expressions,$u^/$ is the velocity in dimensional form, ρ is the fluid density, υ is the kinematic viscosity, D_C is the mass diffusion coefficient, C_p is the heat capacity, and g is the acceleration due to gravity, whileα,β^*, and β are the thermal diffusion, thermal expansion, and the mass expansion coefficients.

Expressions for initial conditions $(t^/ \leq 0)$ suitable for the model are:

$$u^/ = 0, T^/ = T_0, C^/ = C_0 \text{ at } 0 \leq r^/ \leq r_0 \quad (4)$$

Also, boundary conditions $(t^/ > 0)$ for the model are:

$$r^/ = 0, \quad \frac{\partial u^/}{\partial r^/} = \frac{\partial T^/}{\partial r^/} = \frac{\partial C^/}{\partial r^/} = 0$$

$$r^{'} = r_0,\ u^{'} = 0 \begin{Bmatrix} T^/ = T_0 + \frac{(T_w - T_0)t^/\nu}{{r_0}^2\zeta_1} \\ C^/ = C_0 + \frac{(C_w - C_0)t^/\nu}{{r_0}^2\zeta_1} \end{Bmatrix} for\ t^/ < \frac{{r_0}^2\zeta_1}{\nu}$$

$$T^/ = T_w,\ C^/ = C_w \quad for\ \ t^/ \geq \frac{{r_0}^2\zeta_1}{\nu} \quad (5)$$

Appropriate non-dimensional variables are defined as:

$$r = r^{'}/r_0,\ t = t^{'}\nu/{r_0}^2,\ \theta = \frac{T^{'} - T_0}{T_w - T_0},\ \phi = \frac{C^{'} - C_0}{C_w - C_0},\ \text{and } u = \frac{\upsilon u^/}{g\beta^* {r_0}^2(T_w - T_0)} \quad (6)$$

where$r$, t, θ, ϕ, and u are the dimensionless radius, time, temperature, concentration, and velocity, respectively.

Equations (1)-(5) are transformed by the use of (6) into dimensionless form as:

$$\frac{\partial u}{\partial t} = \frac{1}{r}\frac{\partial}{\partial r}\left(r\frac{\partial u}{\partial r}\right) + \theta + N\phi \quad (7)$$

https://doi.org/10.5281/zenodo.17252081

$$\frac{\partial\theta}{\partial t}=\frac{1}{Pr}\left[\frac{1}{r}\frac{\partial}{\partial r}\left(r\frac{\partial\theta}{\partial r}\right)+D_f\frac{1}{r}\frac{\partial}{\partial r}\left(r\frac{\partial\phi}{\partial r}\right)\right]-H\theta \quad (8)$$

$$\frac{\partial\phi}{\partial t}=\frac{1}{Sc}\frac{1}{r}\frac{\partial}{\partial r}\left(r\frac{\partial\phi}{\partial r}\right)-K\phi \quad (9)$$

In equations (7)-(9), $Pr=\upsilon/\alpha$ and $Sc=\upsilon/D$ are the Prandtl number and Schmidt number, respectively. Also, $D_f=D_C(C_w-C_0)/\alpha(T_w-T_0)$, and $N=\beta(C_w-C_0)/\beta^*(T_w-T_0)$ are the Dufour number, and the buoyancy ratio respectively. Finally, $H=Q_0{r_0}^2/\nu\rho C_p$ and $K=K'{r_0}^2/\nu$ are the heat generation/absorption and chemical reaction parameters in the dimensionless form.

Initial and boundary conditions in the dimensionless form are:

For $t\le 0$: $u=0,\theta=0,\phi=0$ at $0\le r\le 1$ (10)

For $t>0$:

$$\left.\begin{aligned} &r=0, && \frac{\partial u}{\partial r}=\frac{\partial\theta}{\partial r}=\frac{\partial\phi}{\partial r}=0\\ &r=1,u=0 && \begin{cases}\theta=\frac{t}{\zeta_1},\phi=\frac{t}{\zeta_1} & for\ t<\zeta_1\\ \theta=1,\phi=1 & for\ \ t\ge\zeta_1\end{cases}\end{aligned}\right\} \quad (11)$$

Using the Heaviside step function, a unified boundary condition of the wall of the tube at $r=1$ for the temperature and concentration can be obtained such that equation (11) becomes:

$$\left.\begin{aligned} &r=0, && \frac{\partial u}{\partial r}=\frac{\partial\theta}{\partial r}=\frac{\partial\phi}{\partial r}=0\\ &r=1,u=0, && \theta=\phi=\frac{1}{\zeta_1}[tH(t)-(t-\zeta_1)H(t-\zeta_1)]\end{aligned}\right\} \quad (12)$$

Let $\bar{u}(s)=\int_0^\infty u(r,t)\exp(-st)dt,\bar{\theta}(s)=\int_0^\infty\theta(r,t)\exp(-st)dt,$ and $\bar{\phi}(s)=\int_0^\infty\phi(r,t)\exp(-st)dt$ be the Laplace transforms of the velocity(u), temperature(θ), and concentration(ϕ). Also, let $\gamma_1=Sc(s+K_r)$, and$\gamma_2=Pr(s+H)$. Then, the governing equations (7)-(9) are transformed as:

$$\frac{1}{r}\frac{d}{dr}\left(r\frac{d\bar{u}}{dr}\right)-s\bar{u}=-\bar{\theta}-N\bar{\phi} \quad (13)$$

$$\frac{1}{r}\frac{d}{dr}\left(r\frac{d\bar{\theta}}{dr}\right)+D_f\frac{1}{r}\frac{d}{dr}\left(r\frac{d\bar{\phi}}{dr}\right)-\gamma_2\bar{\theta}=0 \quad (14)$$

$$\frac{1}{r}\frac{d}{dr}\left(r\frac{d\bar{\phi}}{dr}\right)-\gamma_1\bar{\phi}=0 \quad (15)$$

Equation (14) can further be reduced by the use of equation (15) to:

$$\frac{1}{r}\frac{d}{dr}\left(r\frac{d\bar{\theta}}{dr}\right)+D_f\gamma_1\bar{\phi}-\gamma_2\bar{\theta}=0 \quad (16)$$

Also, equation (12) is converted to the Laplace domain as:

$$\left.\begin{aligned} &\frac{d\bar{u}}{dr}=\frac{d\bar{\theta}}{dr}=\frac{d\bar{\phi}}{dr}=0 && at\ r=0,\\ &\bar{u}=0,\theta=\phi=\frac{1-\exp(-s\zeta_1)}{\zeta_1 s^2} && at\ \ r=1.\end{aligned}\right\} \quad (17)$$

Solutions

Putting$\gamma_3=\frac{1-\exp(-s\zeta_1)}{\zeta_1 s^2}$, the solutions of equations (13), (15), and (16) using (17) are, respectively:

$$\bar{\phi}(r,s)=\gamma_3\frac{I_0(r\sqrt{\gamma_1})}{I_0(\sqrt{\gamma_1})} \quad (18)$$

$$\bar{\theta}(r,s)=\gamma_3\left[\left(1+\frac{\gamma_1 D_f}{\gamma_1-\gamma_2}\right)\frac{I_0(r\sqrt{\gamma_2})}{I_0(\sqrt{\gamma_2})}-\frac{\gamma_1 D_f}{[\gamma_1-\gamma_2)}\frac{I_0(r\sqrt{\gamma_1})}{I_0(\sqrt{\gamma_1})}\right] \quad (19)$$

$$\bar{u}(r,s)=\gamma_3\left[\begin{aligned}&\frac{1}{(\gamma_2-s)}\left(1+\frac{\gamma_1 D_f}{\gamma_1-\gamma_2}\right)\left(\frac{I_0(r\sqrt{s})}{I_0(\sqrt{s})}-\frac{I_0(r\sqrt{\gamma_2})}{I_0(\sqrt{\gamma_2})}\right)\\&+\frac{1}{(\gamma_1-s)}\left(N-\frac{\gamma_1 D_f}{\gamma_1-\gamma_2}\right)\left(\frac{I_0(r\sqrt{\gamma_2})}{I_0(\sqrt{\gamma_2})}-\frac{I_0(r\sqrt{\gamma_1})}{I_0(\sqrt{\gamma_1})}\right)\end{aligned}\right] \quad (20)$$

https://doi.org/10.5281/zenodo.17252081

Isothermal Boundary Conditions:

To highlight the effects of the ramped boundary conditions of the pipe on the fluid flow, it will be meaningful to compare the result with the one with uniform temperature and concentration. Taking into consideration the assumptions made in the previous section, the solutions for fluid temperature, concentration, and velocity for free convection flow in an isothermal pipe can be obtained along the same line as in Jha *et al.* [10] and are presented in the following form

$$\bar{\phi}(r,s) = \frac{I_0(r\sqrt{\gamma_1})}{sI_0(\sqrt{\gamma_1})} \tag{21}$$

$$\bar{\theta}(r,s) = \frac{1}{s}\left[\left(1+\frac{\gamma_1 D_f}{\gamma_1-\gamma_2}\right)\frac{I_0(r\sqrt{\gamma_2})}{I_0(\sqrt{\gamma_2})} - \frac{\gamma_1 D_f}{(\gamma_1-\gamma_2)}\frac{I_0(r\sqrt{\gamma_1})}{I_0(\sqrt{\gamma_1})}\right] \tag{22}$$

$$\bar{u}(r,s) = \frac{1}{s}\left[\begin{array}{l}\frac{1}{(\gamma_2-s)}\left(1+\frac{\gamma_1 D_f}{\gamma_1-\gamma_2}\right)\left(\frac{I_0(r\sqrt{s})}{I_0(\sqrt{s})}-\frac{I_0(r\sqrt{\gamma_2})}{I_0(\sqrt{\gamma_2})}\right)\\ +\frac{1}{(\gamma_1-s)}\left(N-\frac{\gamma_1 D_f}{\gamma_1-\gamma_2}\right)\left(\frac{I_0(r\sqrt{s})}{I_0(\sqrt{s})}-\frac{I_0(r\sqrt{\gamma_1})}{I_0(\sqrt{\gamma_1})}\right)\end{array}\right] \tag{23}$$

Nusselt number(□□), Sherwood number(□□), and Skin friction (□):

Differentiating equations (18)-(20), the Sherwood and Nusselt numbers and the skin friction are respectively given as:

$$\overline{\square h} = \square_3\sqrt{\square_1}\frac{\square_1(\sqrt{\square_1})}{\square_0(\sqrt{\square_1})} \tag{24}$$

$$\overline{\square\square} = \frac{\square\bar{\theta}}{\square\square} = \square_3\left[\left(1+\frac{\square_1\square_\square}{\square_1-\square_2}\right)\frac{\sqrt{\square_2}\square_1(\sqrt{\square_2})}{\square_0(\sqrt{\square_2})} - \left(\frac{\square_1\square_\square}{\square_1-\square_2}\right)\frac{\sqrt{\square_1}\square_1(\sqrt{\square_1})}{\square_0(\sqrt{\square_1})}\right] \tag{25}$$

$$\overline{\square} = -\frac{\square\bar{u}}{\square\square} = \square_3\left[\begin{array}{l}\frac{1}{(\square_2-\square)}\left(1+\frac{\square_1\square_\square}{\square_1-\square_2}\right)\left(\frac{\sqrt{\square}\square_1(\sqrt{\square})}{\square_0(\sqrt{\square})}-\frac{\sqrt{\square_2}\square_1(\sqrt{\square_2})}{\square_0(\sqrt{\square_2})}\right)\\ +\frac{1}{(\square_1-\square)}\left(\square-\frac{\square_1\square_\square}{\square_1-\square_2}\right)\left(\frac{\sqrt{\square}\square_1(\sqrt{\square})}{\square_0(\sqrt{\square})}-\frac{\sqrt{\square_1}\square_1(\sqrt{\square_1})}{\square_0(\sqrt{\square_1})}\right)\end{array}\right] \tag{26}$$

The Laplace Transforms inversion:

The inversion of the Laplace transforms of equations (18)-(26) is difficult. Thus RSA, which is a numerical procedure outlined by Khadrawi and Al-Nimr [13], is applied for the inversion. The inversion is captured as follows:

$$\Pi(\square,\square) = \frac{\square^{\square\square}}{\square}\left[\frac{1}{2}\overline{\Pi}(\square,\square) + \square\square\sum_{\square=1}^{\square}\overline{\Pi}\left(\square,\square+\frac{\square\square\square}{\square}\right)(-1)^{\square}\right] \tag{27}$$

Here, Π represents□, □ and □ in equations (18)-(23), respectively. Furthermore, it means□*h*,□□and □ in (24)-(26), respectively.

Steady state velocity:

The governing equations (7)-(9) are reduced to the steady state ordinary differential equations by eliminating the time derivative (□/□t) and solved analytically to give the velocity as:

$$u(\square) = \frac{1}{\square\square\square}\left(1+\frac{\square_\square\square\square\square_\square}{\square\square\square-\square\square\square}\right)\left(1-\frac{\square_0(\square\sqrt{\square\square\square})}{\square_0(\sqrt{\square\square\square})}\right)+\frac{1}{\square\square\square}\left(\square+\frac{\square_\square\square\square\square_\square}{\square\square\square-\square\square\square}\right)\left(1-\frac{\square_0(\square\sqrt{\square\square\square})}{\square_0(\sqrt{\square\square\square})}\right). \tag{28}$$

Validation:

The numerical values obtained from the exact solution (ES) of equation (28) are presented alongside the numerical values of RSA and a Matlab program, PDEPE, in Table 2 for a comparative study to validate the solution method (RSA).

https://doi.org/10.5281/zenodo.17252081

Results and Discussion:

Figures 2-11 and Table 1 provide an analysis of the transient flow behavior under ramped boundary conditions. These graphical representations illustrate how varying parameters, such as the Prandtl number, Schmidt number, Dufour number, heat source/sink effects, and chemical reactions, affect the concentration, temperature, and velocity fields within the system. Additionally, Table 1 outlines the quantitative effects of these parameters on key performance indicators, such as skin friction, as well as the Nusselt and Sherwood numbers, providing valuable insights into the flow dynamics at work.

In Figures 2–4, the effect of time is to gradually enhance the concentration, temperature, and velocity fields within the vertical tube. Initially, the concentration, temperature, and velocity profiles exhibit small gradients near the walls. As time progresses, diffusion causes the solutal and thermal layers to thicken, which raises the values across the radius and increases the gradients near the walls. This, in turn, heightens the instantaneous fluxes. Consequently, the velocity increases and broadens as buoyancy effects become more significant. At later times, all three profiles converge toward their steady-state conditions, resulting in smoother distributions and stabilized flow. The reference time (t_1) influences these profiles: lowering it increases the profiles, while raising it decreases them.

Figures 5–7 illustrate the effects of the Schmidt number (Sc) and the chemical reaction parameter (K) on the profiles of concentration, temperature, and velocity. A higher Schmidt number (Sc) indicates reduced mass diffusivity, which leads to diminished concentration diffusion and a consequent decrease in concentration levels. This reduction is paired with increased thermal buildup due to suppressed solutal buoyancy, resulting in a rise in temperature while simultaneously decreasing velocity.

In the case of a generative reaction ($K < 0$), the production of solute raises concentration levels, thereby enhancing solutal buoyancy and increasing velocity. However, this increase in velocity comes at the expense of energy consumption, which causes a decrease in temperature. In contrast, a destructive reaction ($K > 0$) produces the opposite effects on these trends.

At high Schmidt numbers, diffusion is significantly limited. As a result, the temperature increase associated with generative reactions is concentrated near the wall, while deeper within the fluid, the effects are reversed due to reduced solute transport.

From Figures 8 and 9, as the Dufour number (D_f) increases, it generates a more pronounced energy flux due to concentration gradients, which enhances heat transfer and raises the temperature profile. This increase in thermal buoyancy leads to higher velocities within the bulk flow. However, near the wall, the Dufour effect has a minimal influence, as the concentration gradients are primarily determined by boundary conditions, making its impact on velocity negligible in that region.

Figures 10-11 illustrate the effects of heat sources or sinks and the Prandtl number on temperature and velocity. When a heat source is present ($Q < 0$), the generation of internal energy raises the fluid temperature, which enhances buoyancy and increases velocity. Conversely, a heat sink ($Q < 0$) absorbs energy, cooling the fluid and weakening the flow.

Additionally, a higher Prandtl number (Pr) decreases thermal diffusivity, which limits heat penetration, resulting in lower temperature and velocity. At high Prandtl numbers, convection remains concentrated near the wall, and the effects of the heat source or sink become minimal toward the center of the tube due to restricted heat diffusion.

Table 1 presents observed trends that clarify the interactions among diffusion, reaction, and buoyancy concerning transport characteristics. Over time, both the Sherwood and Nusselt numbers initially increase as concentration and temperature gradients become more intense. However, they later decline as diffusion layers expand and gradients diminish. Meanwhile, skin friction shows a steady increase,

https://doi.org/10.5281/zenodo.17252081

approaching its limiting value as velocity continues to rise.

A generative reaction improves the solute concentration in the fluid, which decreases mass transfer and subsequently lowers the Sherwood number. In contrast, the increased buoyancy associated with this reaction enhances heat transfer and wall shear, resulting in a higher Nusselt number and increased skin friction. Conversely, a destructive reaction has opposing effects. An increase in the Schmidt number reduces mass diffusivity, leading to a higher Sherwood number. However, this reduction in solutal buoyancy negatively impacts both the Nusselt number and skin friction.

A higher Dufour number intensifies energy flux from concentration gradients, thereby decreasing thermal transfer efficiency and, in turn, lowering the Nusselt number. At the same time, it heightens velocity gradients, which increases skin friction. Similarly, the introduction of a heat source adds energy to the fluid, enhancing buoyancy and skin friction while resulting in a lower Nusselt number. Conversely, a heat sink reverses these effects.

Finally, an increase in the Prandtl number leads to a decrease in thermal diffusivity, which results in more pronounced thermal gradients and a higher Nusselt number, while simultaneously restricting momentum diffusion and lowering skin friction.

Table 2 provides a quantitative comparison of the Riemann Sum Approximation (RSA) method, PDEPE numerical solutions, and Exact Solutions (ES), serving to validate the methodology used in this study. The data shows a close alignment between the results from the RSA method and both the PDEPE and ES across different time and radial values. The discrepancies among the three approaches are minimal, typically within the third or fourth decimal place. This suggests that the RSA method accurately captures flow behavior with high precision confirming that the RSA method is both valid and dependable, as its results are nearly indistinguishable from those of the numerical (PDEPE) and analytical (ES) solutions.

Conclusion:

The analysis shows that transient convection in a vertical tube with ramped thermal and solutal boundaries is highly sensitive to various fluid and system parameters. Over time, the fluid's velocity, temperature, and concentration increase and eventually stabilize at a steady state. Shorter ramp times tend to enhance these profiles. An elevated Schmidt number restricts solute diffusion, which leads to decreased concentration and velocity, although temperature increases. In contrast, a generative reaction improves concentration and velocity but reduces temperature, while a destructive reaction has the opposite effect.

Additionally, the Dufour effect increases energy flux, resulting in higher velocity but lower thermal efficiency. Internal heat generation boosts buoyancy, velocity, and skin friction but simultaneously decreases the Nusselt number. On the other hand, the presence of a heat sink cools the fluid and reduces convection. An increase in the Prandtl number reduces thermal diffusivity, leading to steeper gradients, a higher Nusselt number, and lower velocity.

Overall, these findings highlight that the interactions among diffusion, reaction mechanisms, cross-diffusion, and the effects of heat sources and sinks significantly influence the transient thermofluidic response within the system.

References:

Alharbi, F. M., Alharthi, N. H., & Khan, I. (2023). Thermal radiation effects on unsteady natural convection around a vertical cylinder. Scientific Reports, 13, 12345.

Chamkha, A. J., Rashad, A. M., & Ahmed, S. E. (2011). Heat and mass transfer in chemically reactive fluid flows. International Journal of Heat and Mass Transfer, 54(23-24), 5362–5370. https://doi.org/10.1016/j.ijheatmasstransfer.2011.07.023

Cheng, C. Y. (2010). Soret and Dufour effects on natural convection of a power-law fluid near a vertical cylinder in a porous medium with thermal radiation. International

https://doi.org/10.5281/zenodo.17252081

Communications in Heat and Mass Transfer, 37(8), 1036–1040. https://doi.org/10.1016/j.icheatmasstransfer.2010.10.007

Deka, R. K., & Paul, A. (2012). Transient free convection flow past an infinite moving vertical cylinder in a stably stratified fluid. Journal of Heat Transfer, 134(4), 042503. https://doi.org/10.1115/1.4005205

Deka, R. K., Paul, A., & Chaliha, A. (2017). Transient free convection flow past vertical cylinder with constant heat flux and mass transfer. Ain Shams Engineering Journal, 8(4), 643–651. https://doi.org/10.1016/j.asej.2015.10.006

Deka, R. K., Paul, A., & Sharma, R. (2014). Transient free convection flow past an accelerated vertical circular cylinder in a rotating fluid. Alexandria Engineering Journal, 53(4), 915–922. https://doi.org/10.1016/j.aej.2013.11.005

Dwivedi, N., Bhargava, R., & Sahu, P. (2020). Transient hydromagnetic free convection flow in an infinite vertical cylinder of a second-grade fluid model. Heat Transfer, 49(8), 5036–5056. https://doi.org/10.1002/htj.21818

Dwivedi, N., Bhargava, R., & Sahu, P. (2021). Transient free convection of a second-grade fluid flowing in a vertical cylinder. Heat Transfer, 50(6), 6400–6419. https://doi.org/10.1002/htj.21924

Dwivedi, N., Sahu, P., Bhargava, R., & Kumar, R. (2023). Magneto-nanofluid flow past a vertical cylinder with temperature-dependent heat generation/absorption and chemical reaction. Propulsion and Power Research, 12(1), 128–141. https://doi.org/10.1016/j.jppr.2023.01.011

Ganesan, P., & Rani, H. P. (1998). Transient natural convection along vertical cylinder with heat and mass transfer. Heat and Mass Transfer, 33(5–6), 449–456. https://doi.org/10.1007/s002310050214

Jagan, V., & Sivasankaran, S. (2022). Cross-diffusion at the stationary point over a stretching cylinder. Mathematical and Computational Applications, 27(3), 46. https://doi.org/10.3390/mca27030046

Jha, B. K., Joseph, S. B., & Ajibade, A. O. (2022a). Role of diffusion thermo on unsteady natural convection of a chemically reactive fluid impacted by heat source/sink in a tube. Journal of Taibah University for Science, 16(1), 681–694. https://doi.org/10.1080/16583655.2022.2078135

Jha, B. K., Joseph, S. B., & Ajibade, A. O. (2022b). Effect of chemical reaction, heat source/sink, and thermal diffusion on transient natural convection through a tube. Heat Transfer, 51(8), 4516–4534. https://doi.org/10.1002/htj.22578

Jha, B. K., Oni, M. O. (2016). Natural convection in a vertical tube inspired by time-periodic heating. Alexandria Engineering Journal, 55(2), 1547–1554. https://doi.org/10.1016/j.aej.2016.08.025

Jha, B. K., Oni, M. O., Abba, J. M., & Mundi, B. I. (2024). Unsteady natural convection flow in a vertical tube inspired by ramped surface heating. International Journal of Magnetics and Electromagnetism, 10(1), 1–13. https://doi.org/10.35840/2631-5068/6543

Jha, B. K., Samaila, A. K., & Ajibade, A. O. (2011). Transient free-convective flow of reactive viscous fluid in a vertical tube. Mathematical and Computer Modelling, 54(11–12), 2880–2888. https://doi.org/10.1016/j.mcm.2011.07.008

Khan, I., Ali, F., Bin-Mahfouz, A., & Alqahtani, A. M. (2018). Natural convection heat transfer in an oscillating vertical cylinder. PLOS ONE, 13(12), e0188656. https://doi.org/10.1371/journal.pone.0188656

Machireddy, G. R. (2013). Chemically reactive species and radiation effects on MHD convective flow past a moving vertical cylinder. Ain Shams Engineering Journal, 4(4), 879–888. https://doi.org/10.1016/j.asej.2013.04.003

Mahato, R., Das, M. M., & Sibanda, P. (2021). Hall effect on MHD transient free convection of a chemically reactive Casson fluid with heat source/sink past an infinite vertical cylinder. Physica Scripta, 96(1), 015207. https://doi.org/10.1088/1402-4896/abc5eb

Paul, A., Deka, R. K., & Chaliha, A. (2017). Unsteady natural convection flow past an infinite vertical circular cylinder in a stratified fluid. Mathematical Problems in Engineering,

2017, 8410691. https://doi.org/10.1155/2017/8410691

Rani, H. P. (2003). Transient natural convection along a vertical cylinder with variable surface temperature and mass diffusion. Heat and Mass Transfer, 40(1–2), 67–73. https://doi.org/10.1007/s00231-002-0372-1

Rani, H. P., & Kim, K.-Y. (2009). Dufour and Soret effects on unsteady natural convection flow past an isothermal vertical cylinder. Korean Journal of Chemical Engineering, 26(6), 1573–1580. https://doi.org/10.1007/s11814-009-0158-y

Rani, H. P., & Reddy, G. J. (2013). Soret and Dufour effects on unsteady MHD free convection along a vertical cylinder in a couple stress fluid. Journal of Applied Fluid Mechanics, 6(2), 199–206. https://doi.org/10.29252/jafm.06.02.244

Shaheen, N., Alshehri, H. M., Ramzan, M., Shah, Z., Alrabaiah, H., Kumam, P., & Nisar, K. S. (2021). Soret and Dufour effects on a Casson nanofluid flow past a deformable cylinder with variable characteristics and Arrhenius activation energy. Scientific Reports, 11, 19282. https://doi.org/10.1038/s41598-021-98898-6

Sravanthi, C. S., Reddy, E. K., & Rao, V. R. (2018). Slip flow of nanofluid over a stretching vertical cylinder in a porous medium with non-linear thermal radiation and heat source/sink. Scientia Iranica, 25(2), 654–667. https://scientiairanica.sharif.edu/article_4580.html

Vanita, A., & Kumar, V. (2016). Effect of radial magnetic field on free convective flow over a ramped-velocity moving vertical cylinder with ramped-type temperature and concentration. Journal of Applied Fluid Mechanics, 9(6), 2855–2864. https://doi.org/10.29252/jafm.09.06.26060

Figure 1: Display of the physical problem

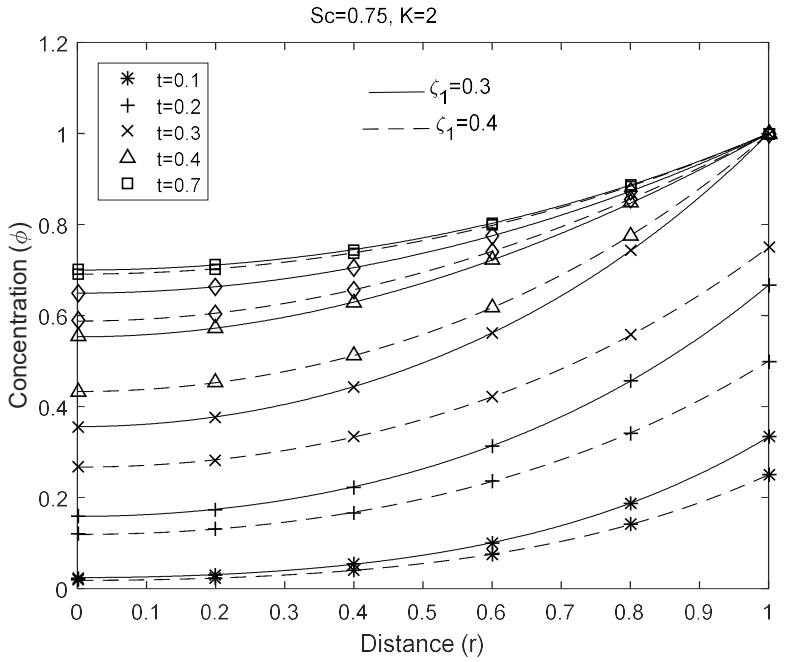

Figure 2: Ramped concentration profiles for different □ and□ *1*

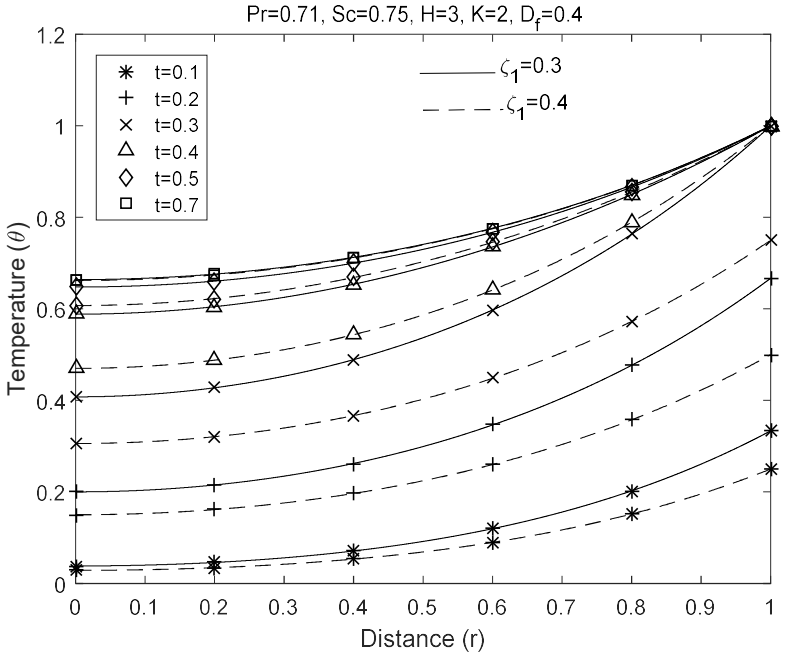

Figure 3: Ramped temperature profiles for different □ and□ *1*

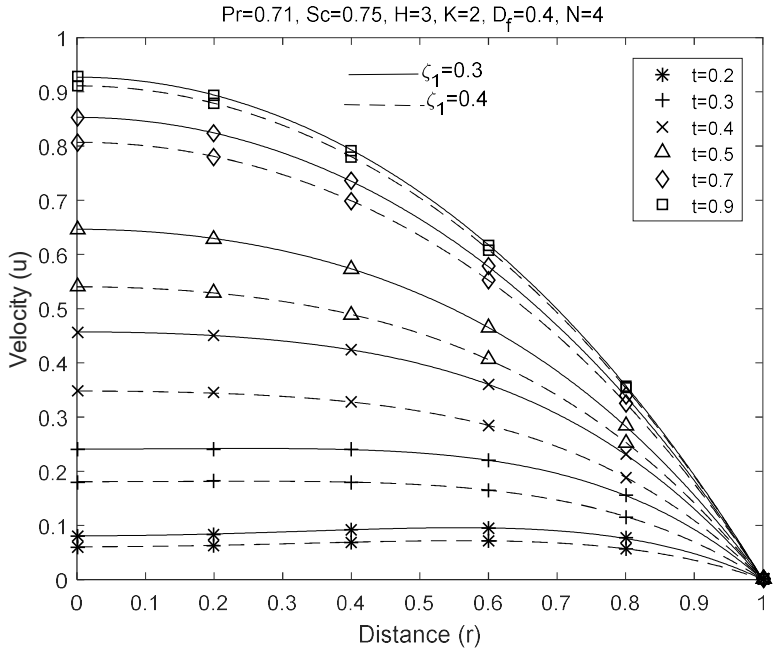

Figure 4: Ramped velocity profiles for different □ and□ *1*

https://doi.org/10.5281/zenodo.17252081

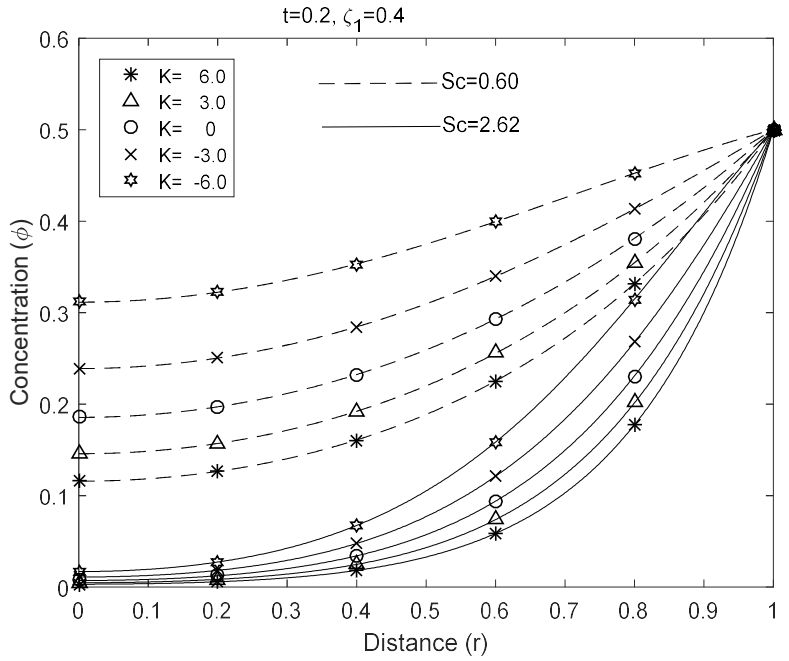

Figure 5: Effect of □ and □□ on the concentration profiles

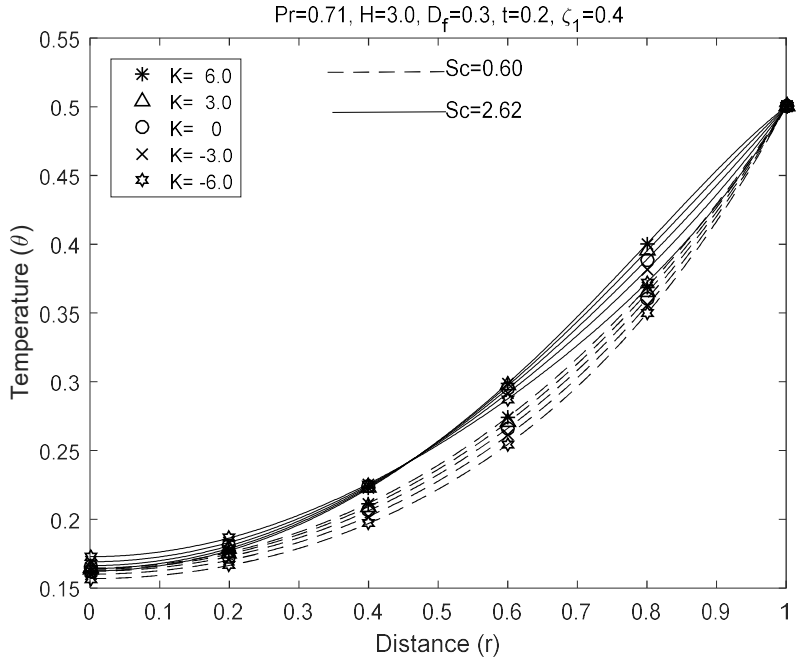

Figure 6: Effect of □ and □□ on the temperature profiles

https://doi.org/10.5281/zenodo.17252081

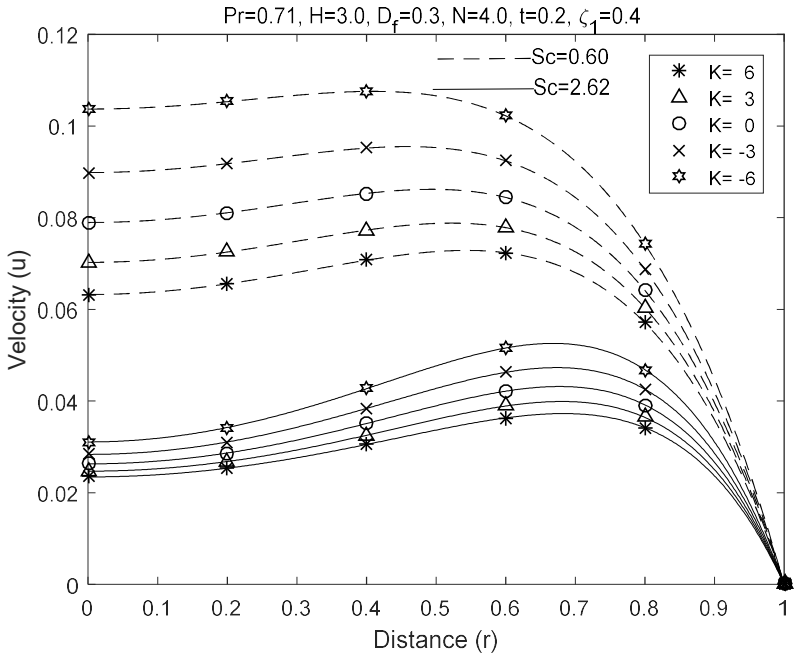

Figure 7: Effect of □ and □□ on the velocity profiles

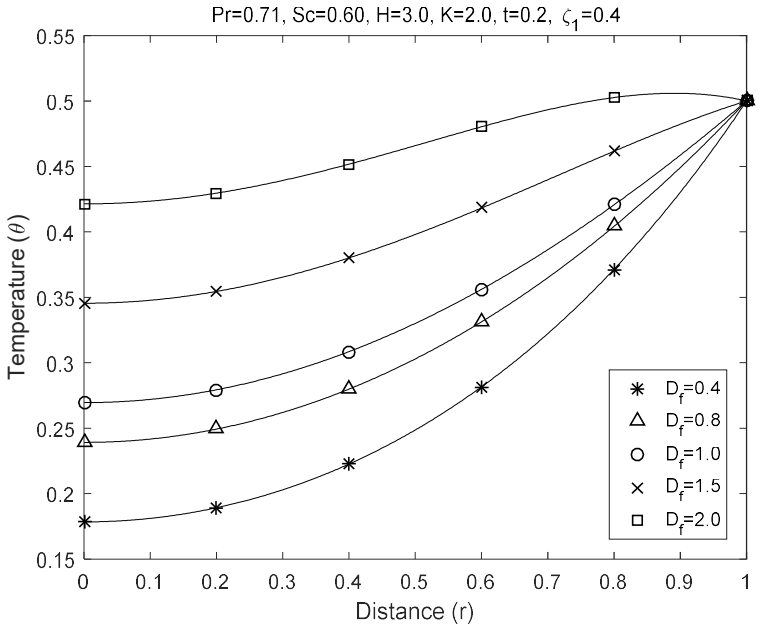

Figure 8: Influence of Dufour number on the temperature profiles

https://doi.org/10.5281/zenodo.17252081

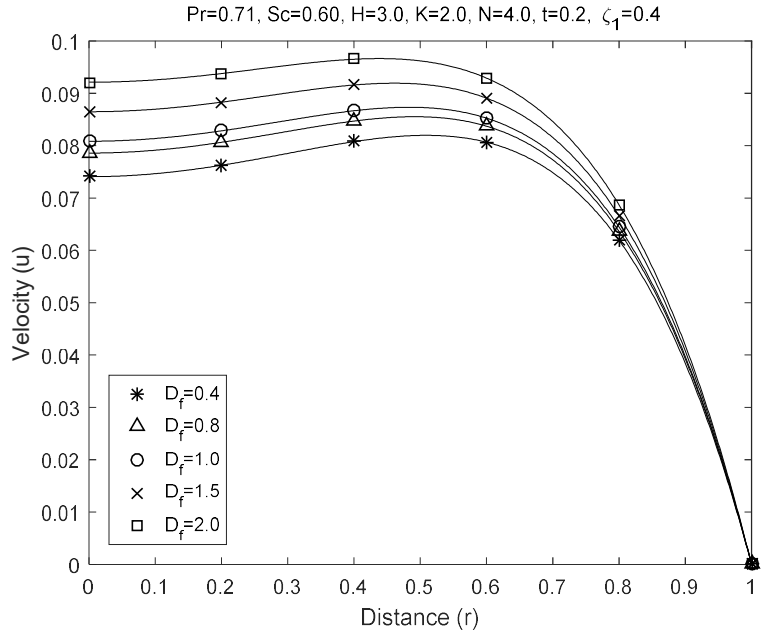

Figure 9: Impact of Dufour number on the velocity profiles

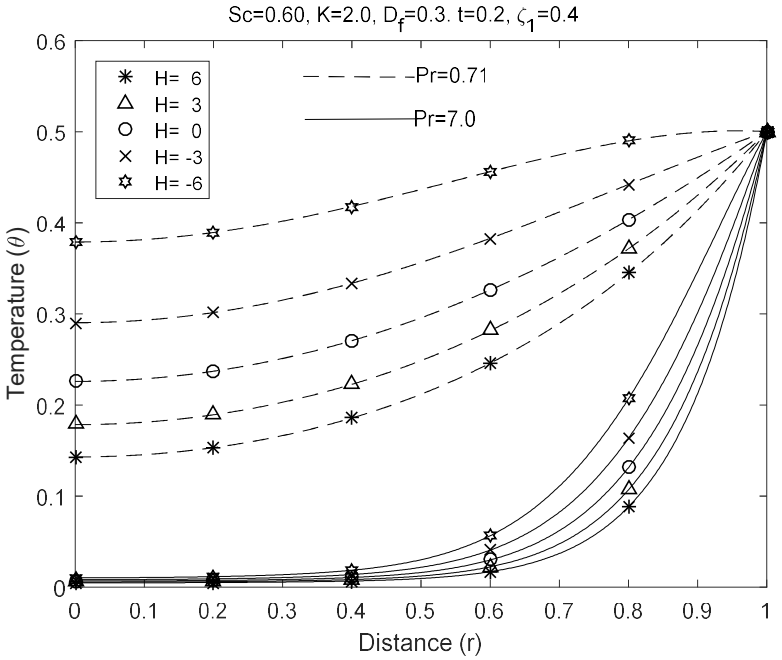

Figure 10: Effect of heat source/sink and Prandtl number on the temperature profiles

https://doi.org/10.5281/zenodo.17252081

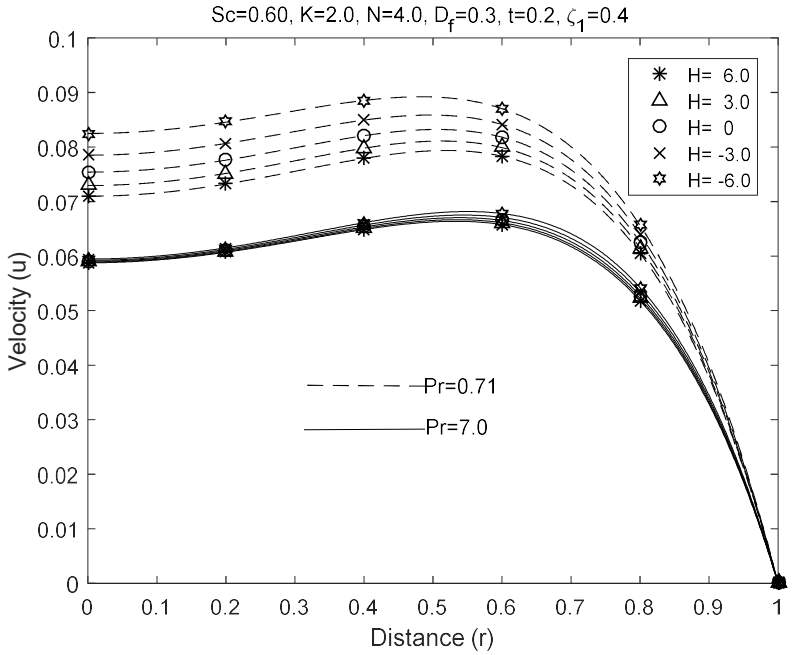

Figure 11: Effect of heat source/sink and Prandtl number on the velocity profiles

Table 1: Effect of the flow parameters on □*h*, □□ and □ with ramped boundary conditions (□ = 0.3, □ = 2.0, □ = 4.0, □□ = 0.4, □1 = 0.4, □ = 4.0)

Variable		*Sh*	*Nu*	*τ*	**Variable**		*Nu*	*τ*
	0.2	0.8058	0.8119	0.4738		0.4	0.7574	0.4758
	0.3	0.9609	1.0038	0.8700		0.8	0.5394	0.4842
t	0.4	1.0899	1.1778	1.3256	D_f	1	0.4304	0.4883
	0.5	0.6358	0.7877	1.6505		1.5	0.1580	0.4988
	0.8	0.5287	0.7272	2.0632		2	-0.1145	0.5092
	1.9	0.5250	0.7272	2.1652		6	1.0109	0.4689
	Steady-state	0.5249	0.7272	2.1652		3	0.8119	0.4738
	6	1.0400	0.7618	0.4510	*H*	0	0.5878	0.4795
	3	0.8675	0.7989	0.4676		-3	0.3310	0.4864
K	0	0.6747	0.8388	0.4871		-6	0.0308	0.4946
	-3	0.4555	0.8818	0.5101	Pr	0.71	0.8119	0.4738
	-6	0.2015	0.9289	0.5377		7	3.6386	0.4226
Sc	0.60	0.8058	0.8119	0.4738				
	2.62	2.0396	0.5189	0.3483				

https://doi.org/10.5281/zenodo.17252081

Table 2: Numerical comparison of Riemann sum approximation method (□□□) solutions, □□□□□ and steady-state exact solutions (□□)(□□ = *0.71*, □□ = *0.60*, □ = *3*, □ = *2*, □□ = *0.2*, □ = *4*, □1 = *0.4*)

		Velocity				**Velocity**		
□	□	□□□	□□□□□	□	□	□□□	□□□□□	□□
0.2	0	0.0718	0.0720	0.6	0	0.7505	0.7507	
	0.2	0.0741	0.0742		0.2	0.7277	0.7279	
	0.4	0.0788	0.0785		0.4	0.6555	0.6558	
	0.6	0.0791	0.0784		0.6	0.5226	0.5230	
	0.8	0.0611	0.0603		0.8	0.3116	0.3120	
0.4	0	0.3856	0.3856	2.0	0	0.9986	1.0045	0.9985
	0.2	0.3799	0.3799		0.2	0.9617	0.9674	0.9616
	0.4	0.3584	0.3583		0.4	0.8495	0.8545	0.8494
	0.6	0.3070	0.3067		0.6	0.6575	0.6614	0.6574
	0.8	0.2003	0.2001		0.8	0.3781	0.3803	0.3780

https://doi.org/10.5281/zenodo.17252081